J|A|C|S
ARTICLES
Published on Web 03/05/2004

Covalent versus Electrostatic Nature of the Strong Hydrogen Bond: Discrimination among Single, Double, and Asymmetric Single-Well Hydrogen Bonds by Variable-Temperature X-ray Crystallographic Methods in β-Diketone Enol RAHB Systems

Paola Gilli, Valerio Bertolasi, Loretta Pretto, Valeria Ferretti, and Gastone Gilli*

Contribution from the Centro di Strutturistica Diffrattometrica and Dipartimento di Chimica, Universitá di Ferrara, Via L. Borsari, 46, 44100 Ferrara, Italy

Received April 7, 2003; Revised Manuscript Received January 8, 2004; E-mail: ggilli.chim@unife.it.

Abstract: β-Diketone enols are known to form intramolecular ···O=C−C=C−OH··· resonance-assisted hydrogen bonds (RAHBs) with O···O distances as short as 2.39−2.44 Å. However, even the most accurate diffraction studies have not been able to assess with certainty whether these very strong hydrogen bonds (H-bonds) are to be described as proton-centered O···H···O bonds in a single-well (SW) potential or as the dynamic or static mixing of two O−H···O ⇌ O···H−O tautomers in a double-well (DW) one. This contribution reexamines the problem and shows that diffraction methods are fairly able to assess the SW or DW nature of the H-bond formed and, in the second case, its dynamic or static nature, provided a Bayesian approach is used which associates a number of experimental techniques (X-ray crystallography at variable temperature, difference Fourier maps, least-squares refinement of proton populations, Hirshfeld's rigid-bond test) with a reasonable *prior*, that is the full set of possible proton-transfer (PT) pathways for the O−H···O system derived from theoretical calculations. The method is first applied to three β-diketone enols, whose crystal structures were determined in the interval of temperatures 100−295 K and then generalized to the interpretation of a much wider set of β-diketone enol structures derived from the literature, making it possible to establish a general relationship between chemical structure (symmetric or dissymmetric substitution, steric compression or stretching, increased π-bond delocalizability), H-bond strength, and the shape of the PT-barrier. Final results are interpreted in terms of simplified VB theory and state-correlation (or avoided-crossing) diagrams.

Introduction

Although the well-known fact that X−H···Y hydrogen bonds (H-bonds) are "formed only between the most electronegative atoms"[1] may suggest an electrostatic origin for this interaction, it is now widely recognized that the forces determining H-bond strength are a mixture of both electrostatic and covalent contributions, that the covalent part is steeply increasing while the difference of proton affinities, $\Delta PA = PA(X^-) - PA(Y)$, or acidity constants, $\Delta pK_a = pK_a(X-H) - pK_a(H-Y^+)$, is approaching zero, and that, when this limit is achieved, very strong and symmetrical X···H···Y bonds are formed which are better classified as three-center-four-electron covalent bonds, that is a 1:1 mixture of the two X−H···Y ↔ X···H−Y VB resonance forms. This is, essentially, the conclusion of the qualitative electrostatic-covalent H-bond model (ECHBM)[2] in agreement with a wealth of experimental and theoretical evidence concerning the covalent nature of very strong H-bonds[3,4] and the essential role played by PA/pK_a matching.[5]

(1) Pauling, L. *The Nature of the Chemical Bond*, 3rd ed.; Cornell University Press: Ithaca, NY, 1960.

(2) (a) Gilli, P.; Bertolasi, V.; Ferretti, V.; Gilli, G. *J. Am. Chem. Soc.* **1994**, *116*, 909. (b) Gilli, G.; Gilli, P. *J. Mol. Struct.* **2000**, *552*, 1. (c) Gilli, P.; Bertolasi, V.; Ferretti, V.; Gilli, G. *J. Am. Chem. Soc.* **2000**, *122*, 10405. (d) Gilli, P.; Bertolasi, V.; Pretto, L.; Lyčka, A.; Gilli, G. *J. Am. Chem. Soc.* **2002**, *124*, 13554. (e) Gilli, G.; Gilli, P. In *Strength from Weakness: Structural Consequences of Weak Interactions in Molecules, Supermolecules, and Crystals*; Domenicano, A., Hargittai, I., Eds.; Kluwer: Dordrecht, 2001; Chapter 14.

(3) (a) Pimentel, G. C. *J. Chem. Phys.* **1951**, *19*, 446. (b) Stevens, E. D.; Lehmann, M. S.; Coppens, P. *J. Am. Chem. Soc.* **1977**, *99*, 2829. (c) Flensburg, C.; Larsen, S.; Stewart, R. F. *J. Phys. Chem.* **1995**, *99*, 10130. (d) Madsen, D.; Flensburg, C.; Larsen, S. *J. Phys. Chem. A* **1998**, *102*, 2177. (e) Madsen, G. K. H.; Iversen, B. B.; Larsen, F. K.; Kapon, M.; Reisner, G. M.; Herbstein, F. H. *J. Am. Chem. Soc.* **1998**, *120*, 10040. (f) Schiøtt, B.; Iversen, B. B.; Madsen, G. H. K.; Bruice, T. C. *J. Am. Chem. Soc.* **1998**, *120*, 12117. (g) Jaskólski, M.; Olovsson. I.; Tellgren, R.; Mickiewicz-Wichłacz; D. *Acta Crystallogr.* **1982**, *B38*, 291. (h) Cotton, F. A.; Fair, C. K.; Lewis, G. E.; Mott, G. N.; Ross, F. K.; Schultz, A. J.; Williams, J. M. *J. Am. Chem. Soc.* **1984**, *106*, 5319.

(4) (a) Coulson, C. A.; Danielsson, U. *Ark. Fys.* **1954**, *8*, 239. (b) Coulson, C. A.; Danielsson, U. *Ark. Fys.* **1954**, *8*, 245. (c) Reid, C. *J. Chem. Phys.* **1959**, *30*, 182. (d) Kollman, P. A.; Allen, L. C. *J. Am. Chem. Soc.* **1970**, *92*, 6101. (e) Desmeules, P. J.; Allen, L. C. *J. Chem. Phys.* **1980**, *72*, 4731. (f) Dannenberg, J. J.; Haskamp, L.; Masunov, A. *J. Phys. Chem. A* **1999**, *103*, 7083. (g) Fuster, F.; Silvi, B. *Theor. Chem. Acc.* **2000**, *104*, 13. (h) Gatti, C.; Cargnoni, F.; Bertini, L. *J. Comput. Chem.* **2003**, *24*, 422. (i) Garcia-Viloca, M.; González-Lafont, A.; Lluch, J. M. *J. Am. Chem. Soc.* **1997**, *119*, 1081.

(5) (a) Meot-Ner (Mautner), M. *J. Am. Chem. Soc.* **1984**, *106*, 1257. (b) Meot-Ner (Mautner), M. In *Molecular Structure and Energetics*; Liebman, J. F., Greenberg, A., Eds.; VCH: Weinheim, 1987; Vol. IV, Chapter 3. (c) Zeegers-Huyskens, T. *J. Mol. Struct.* **1986**, *135*, 93. (d) Zeegers-Huyskens, T.; Huyskens, P. L. In *Intermolecular Forces*; Huyskens, P. L., Luck, W. A., Zeegers-Huyskens, T., Eds.; Springer-Verlag: Berlin, 1991; Chapter 1. (e) Zeegers-Huyskens, T. In *Intermolecular Forces*; Huyskens, P. L., Luck, W. A., Zeegers-Huyskens, T., Eds.; Springer-Verlag: Berlin, 1991; Chapter 6. (f) Malarski, Z.; Rospenk, M.; Sobczyk, L.; Grech, E. *J. Phys. Chem.* **1982**, *86*, 401. (g) Sobczyk, L. *Ber. Bunsen-Ges. Phys. Chem.* **1998**, *102*, 377. (h) Pan, Y.; McAllister, M. A. *J. Org. Chem.* **1997**, *62*, 8171.

Moreover, extensive analysis of crystal structures of H-bonded compounds[2] has shown that these very strong H-bonds can only occur in connection with four very specific molecular patterns to which we have often made reference to as "chemical leitmotifs".[2e] The first of them, hereafter called (±)CAHB or *positive/negative charge-assisted H-bond*,[2b] concerns the association of acid−base pairs with natural PA/pK_a matching that can easily exchange the proton, giving rise to very strong and nearly symmetric X···H···Y bonds. These bonds are rather rare, and among the very few studied by accurate neutron diffraction methods, we may quote pentachlorophenol−pyridine[6a] (N···O = 2.513(3) Å at 100 K; $\Delta pK_a \simeq -0.8$), pyridine-*N*-oxide−trichloroacetic acid[6b,c] (O···O = 2.430(2) Å at 120 K; $\Delta pK_a \simeq -0.1$) and urea−phosphoric acid[6d] (O···O = 2.400(5) Å at 150 K; $\Delta pK_a \simeq 2.0$) complexes. On the contrary, in more ordinary H-bonds the PA/pK_a difference between the H-bond donor and acceptor groups is normally very large as, for instance, in water HOH···OH_2 dimers **Ia** ($\Delta pK_a = pK_a(HO-H) - pK_a(H^+-OH_2) = 15.74 - (-1.74) = 17.48$) or in alcohol−ketone ROH···O=CR_2 complexes **IIa** ($\Delta pK_a = pK_a(RO-H) - pK_a(H^+-O=CR_2) = (15 \div 18) - (-6 \div -7) = 21 \div 25$) which, accordingly, can both form only rather weak electrostatic H-bonds with typical O···O distances of 2.70−2.85 Å. However, molecules forming *homonuclear* H-bonds can overcome the PA/pK_a difference by other artifices able to turn weak X−H···X electrostatic bonds into strong and symmetric X···H···X covalent interactions. Inspection of crystal structures of molecules forming strong or very strong homonuclear H-bonds (in particular O−H···O[2a]) has shown that these further leitmotifs are only three: (i) (+)CAHB or *positive-charge-assisted H-bond*, $[X\cdots H\cdots X]^+$; (ii) (−)CAHB or *negative-charge-assisted H-bond*, $[X\cdots H\cdots X]^-$; and (iii) R_n−RAHB or *resonance-assisted H-bond*,[7] where the H-bond donor and acceptor atoms are connected by a π-conjugated R_n fragment of *n* atoms (*n* odd). The mechanisms of $\Delta PA/\Delta pK_a$ annihilation are clearly seen with reference to the two O−H···O examples given above. The water dimer **Ia** ($\Delta pK_a = 17.48$) is transformed by proton removal into the $[H-O\cdots H\cdots O-H]^-$ hydroxyl−water complex **Ib** ($\Delta pK_a = pK_a(HO-H) - pK_a(H-OH) = 0$; range of O···O distances in $[O\cdots H\cdots O]^-$ bonds = 2.36−2.49 Å)[2a] or, by proton addition, into the $[H_2O\cdots H\cdots OH_2]^+$ hydronium−water complex **Ic** ($\Delta pK_a = pK_a(H_2O-H^+) - pK_a(H^+-OH_2) = 0$; range of O···O distances in $[O\cdots H\cdots O]^+$ bonds = 2.36−2.43 Å)[2a]. Analogously, the rather weak ROH···O=CR_2 alcohol−ketone complex **IIa** ($\Delta pK_a = 21-25$) can be made much stronger by connecting the two oxygens by an R_3 conjugated group, which transforms it into a β-diketone enol **IIb** whose two equally probable ···O=C−C=C−OH··· and ···HO−C=C−C=O··· resonance forms would naturally lead to a $\Delta pK_a = 0$ whenever the full π-delocalization is reached (**IIb**; range of O···O distances in β-diketones: intramolecular 2.43−2.55, intermolecular 2.46−2.65 Å).[2a]

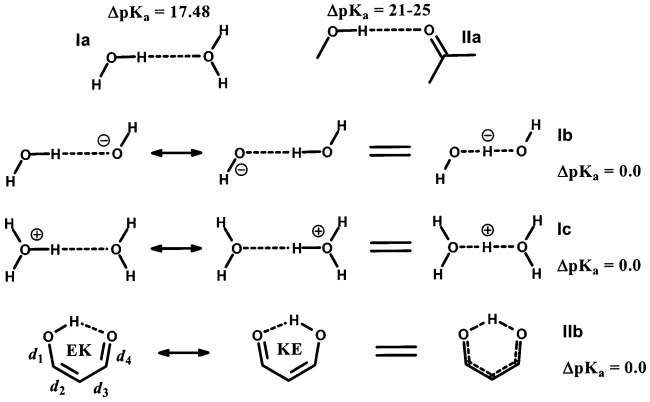

The occurrence of strong, nearly proton-centered and essentially covalent H-bonds due to $\Delta PA/\Delta pK_a$ equalization has been experimentally proved for the three types of charge-assisted H-bonds [(±)CAHB,[6a−d] (−)CAHB,[3b−d] and (+)CAHB[3g,h]] by neutron crystallographic methods. Conversely, the formation of such strong and centered bonds in RAHB remains controversial despite the many studies carried out on O−H···O RAHBs by sophisticated experimental techniques such as microwave spectroscopy,[6g] neutron diffraction,[6f,h] and combined X-ray and neutron deformation densities.[3e] Uncertainties derive from the difficulty in distinguishing between genuine proton centering within a single-well potential and the result of dynamic or static disorder of the proton experiencing a double-well potential without having any a priori knowledge of the shapes that the proton-transfer (PT) pathway can adopt in H-bonds of different strengths.

The idea that the a priori knowledge of the possible pathways (*the prior*) can contribute to obtain a better interpretation of the experimental findings (*the posterior*) derives from the Bayes theorem, which is briefly discussed in note,[8] while our capability of obtaining a *prior* able to predict the shapes of PT-pathways and barriers derives from a recent paper[2d] which has clarified the general relationships between them and the strength of the H-bond by applying Hammond postulate[9a] and Marcus rate-

(6) (a) Steiner, Th.; Majers, I.; Wilson, C. C. *Angew. Chem., Int. Ed.* **2001**, *40*, 2651. (b) Golič, L.; Hadži, D.; Lazarini, F. *J. Chem. Soc., Chem. Commun.* **1971**, 460. (c) Eichhorn, K. D. *Z. Kristallogr.* **1991**, *195*, 205. (d) Wilson, C. C. *Acta Crystallogr.* **2001**, *B57*, 435. (e) Boese, R.; Antipin, M. Yu.; Bläser, D.; Lyssenko, K. A. *J. Phys. Chem. B* **1998**, *102*, 8654. (f) Madsen, G. K. H.; Wilson, C.; Nymans, Th. M.; McIntyre, G. J.; Larsen, F. K. *J. Phys. Chem. A* **1999**, *103*, 8684. (g) Baughcum, S. L.; Duerst, R. W.; Rowe, W. F.; Smith, Z.; Bright Wilson, E. *J. Am. Chem. Soc.* **1981**, *103*, 6296. (h) Jones, R. D. G. *Acta Crystallogr.* **1976**, *B32*, 1807.

(7) (a) Gilli, G.; Bellucci, F.; Ferretti, V.; Bertolasi, V. *J. Am. Chem. Soc.* **1989**, *111*, 1023. (b) Bertolasi, V.; Gilli, P.; Ferretti, V.; Gilli, G. *J. Am. Chem. Soc.* **1991**, *113*, 4917. (c) Gilli, G.; Bertolasi, V.; Ferretti, V.; Gilli, P. *Acta Crystallogr.* **1993**, *B49*, 564. (d) Bertolasi, V.; Gilli, P.; Ferretti, V.; Gilli, G. *Chem. Eur. J.* **1996**, *2*, 925. (e) Gilli, P.; Ferretti, V.; Bertolasi, V.; Gilli, G. In *Advances in Molecular Structure Research*; Hargittai, I., Hargittai, M., Eds.; JAI Press Inc.: Greenwich, CT, 1996; Vol. 2, p 67. (f) Gilli, P.; Ferretti, V.; Gilli, G. In *Fundamental Principles of Molecular Modeling*; Gans, W., Amann, A., Boeyens, J. C. A., Eds.; Plenum Press: New York, 1996.

(8) Bayes's theorem, on which Bayesian statistics is based (Molina, E. C. *Two Papers by Bayes with Commentaries*; Hafner Publishing Company: New York, 1963) has received increasing attention in the past decade as a tool for data treatment and interpretation which can take advantage of all a priori information available for a better understanding of experimental results (Sivia, D. S. *Data Analysis. A Bayesian Tutorial*; Oxford University Press: Oxford, 2003; Gilmore, C. J. *Acta Crystallogr.* **1996**, *A52*, 561). In the present case, it can be written as p(PT-pathway|Data) ∝ p(Data|PT-pathway)·p(PT-pathway) where p = probability of; p(PT-pathway) = *prior* = what we already know about the distribution function of the possible PT-pathways (described after the Introduction); p(Data|PT-pathway) = *likelihood* = what we predict to be the experimental results for any given pathway; p(PT-pathway|Data) = *posterior* = our new knowledge of the distribution function of the possible PT-pathways updated with respect to the *prior* by means of the new experimental results collected. The *posterior* is assumed to become an updated *prior* for future studies. Table of *likelihoods*, that is the results of the different tests expected for the PT-pathways of the *prior*, is given in Table S5 of Supporting Information.

(9) (a) Hammond, G. S. *J. Am. Chem. Soc.* **1955**, *77*, 334. (b) Marcus, R. A. *Discuss. Faraday Soc.* **1960**, *29*, 21. (c) Marcus, R. A. *J. Phys. Chem.* **1968**, *72*, 891. (d) Shaik, S. S.; Schlegel, H. B.; Wolfe, S. *Theoretical Aspects of Physical Organic Chemistry. The S_N2 Mechanism*; John Wiley: New York, 1992. (e) Grunwald, E. *J. Am. Chem. Soc.* **1985**, *107*, 125.

equilibrium theory[9b−e] to DFT-calculated PT-pathways of a series of N−H···O/O−H···N RAHB-forming ketohydrazones.

Accordingly the present report starts by describing a complete set of PT-pathways and barriers that can be reasonably predicted for the O−H···O bond system (summarized in schemes **III**−**VI**) and, in a second time, makes use of this information as a *prior* to interpret the crystal structures of a number of β-diketone enol derivatives forming O−H···O RAHBs, **IIb**, with the aim of establishing how their geometries and PT features are affected by different factors, such as steric effects or dissymmetric substitution. The experimental method used is variable-temperature X-ray crystallography as the method of election to measure proton populations (or occupancies) in the solid state and then to assess the qualitative features of PT-pathways. Compounds investigated are (2*Z*)-1-(4-methoxyphenyl)-3-(3-nitrophenyl)-1,3-propanedione enol (**A**), 2,2′-ethylenebis(1,3-cyclohexanedione enol) (**B**) and (2*Z*)-3-mesityl-1-(2-nitrophenyl)-1,3-propanedione enol (**C**), whose crystal structures were previously determined in our laboratory at room temperature,[7b,d] suggesting the possibility that they might span the complete range of the PT-pathways of interest. The analysis is then extended to all crystal structures of similar molecules of sufficient accuracy retrieved from the Cambridge Structural Database (CSD).[10] Finally, it is shown that the results obtained can be consistently interpreted in terms of simplified VB theory and state-correlation (or avoided crossing) diagrams.

The Prior: Predicted PT-Profiles for the O−H···O Bond

Schemes **III**−**VI** illustrate the shapes of the possible O−H···O PT-pathways in the form of E_{HB} versus *RC* plots, where E_{HB} is the energy of the H-bond and $RC = [d(O-H) - d(H\cdots O)]$ is the reaction coordinate, which is zero only for the perfectly proton-centered bond. Profiles have been calculated by semiempirical methods over a wide range of H-bond strengths (i.e. O···O distances) and symmetries by the use of the Lippincott and Schroeder force-field for the O−H···O bond.[11] Their interpretation strictly follows the criteria previously detailed for the N−H···O/O−H···N RAHB[2d]. As for the nomenclature used, PT-pathways are called *single-minimum* (SM) (**1**, **1a**,**b**) or *double-minimum* (DM) (**2**, **2a**,**b**, **3**, **4**, **4a**−**d**) according to whether their analytical profile has one or two minima, and *single-well* (SW) (**1**, **1a**,**b**, **2**, **2a**,**b**, **4c**,**d**) or *double-well* (DW) (**3**, **4**, **4a**,**b**) according to whether the proton is experimentally observed in a single position or in two positions with partial populations $p_1 + p_2 = 1$. SW pathways are further distinguished according to their *RC* value in *symmetric* (sSW) (**1**, **2**), *weakly asymmetric* (waSW) (**1a**,**b**, **2a**,**b**), and *asymmetric* (aSW) (**4c**,**d**), while DW ones are classified as *symmetric* (sDW) (**3**, **4**) when $p_1 = p_2 = {}^1/_2$ and $\Delta E_{1-2} = 0$ or *asymmetric* (aDW) (**4a**,**b**) when $p_1 \neq p_2$ and $\Delta E_{1-2} \neq 0$, where ΔE_{1-2} is the difference between the zero vibrational levels of the two minima (see **VI**). The PT-barrier, measured by the energy barrier $\Delta E^{\ddagger}$ (**VI**), is indicated as *no-barrier* (NB) when it is lower than the proton vibrational level (**1**, **1a**,**b**, **2**, **2a**,**b**), *low-barrier* (LB) when its easy crossing produces dynamically disordered crystals (**3**), and *high-barrier* (HB) when it cannot be easily crossed, thus giving origin to statically disordered (**4**, **4a**,**b**) or perfectly ordered (**4c**,**d**) crystals. Both SW and DW *symmetrical* pathways and barriers are called *intrinsic* according to the Marcus treatment.[9b−e] H-bonds formed in these two cases are called *intrinsic H-bonds* as well; they occur when $\Delta PA/\Delta pK_a = \Delta E_{1-2} = 0$ and are, by definition, the strongest H-bonds possible in any specific D−H···A H-bonded system, in the sense that uneven chemical substitution can only increase $\Delta PA/\Delta pK_a$ and then weaken the H-bond formed.[2d] This nomenclature bears only indirect relationships with that used in enzymology studies[12] which make use of the acronyms LBHB (low-barrier H-bond) or SSHB (short-strong H-bond) to indicate H-bonds plausibly

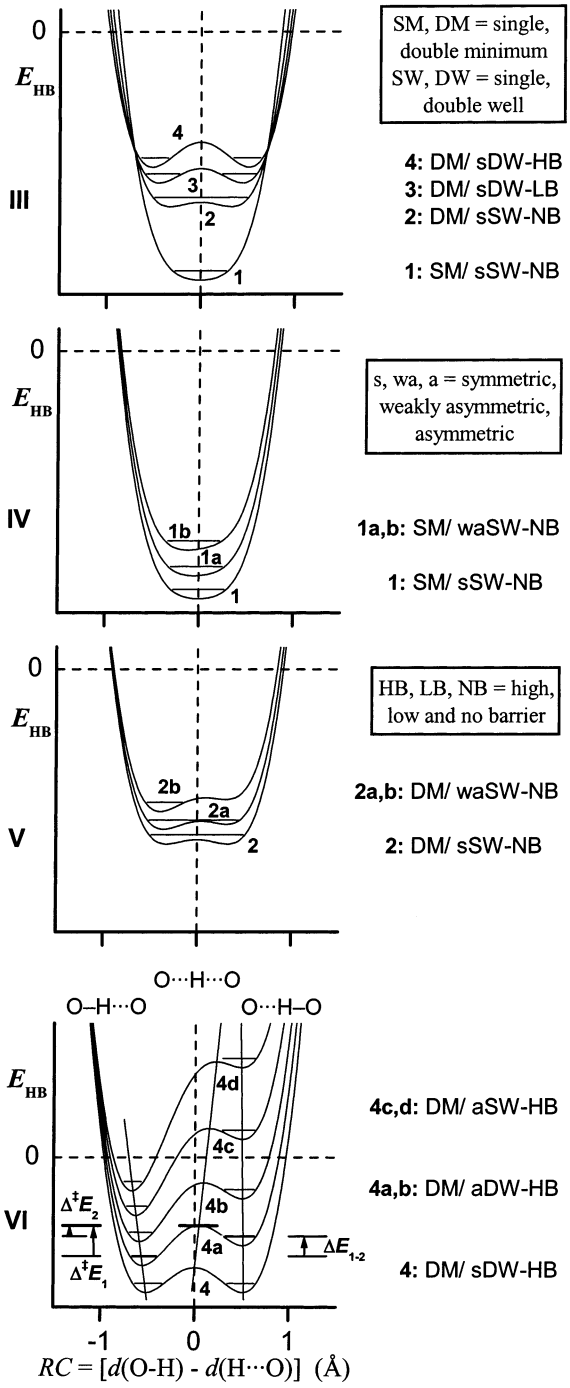

(10) Allen, F. H.; Bellard, S.; Brice, M. D.; Cartwright, B. A.; Doubleday: A.; Higgs, H.; Hummelink, T.; Hummelink-Peters, B. G.; Kennard, O.; Motherwell, W. D. S.; Rodgers, J.; Watson, D. G. *Acta Crystallogr*. **1979**, *B35*, 2331.

(11) (a) Lippincott, E. R.; Schroeder, R. *J. Chem. Phys.* **1955**, *23*, 1099. (b) Schroeder, R.; Lippincott, E. R. *J. Phys. Chem.* **1957**, *61*, 921.

Table 1. H-Bond Parameters (Å and deg), H−Bond Proton Populations (p(%)), Bond Distances of the Conjugated HO−C═C−C═O Fragment, d_1-d_4 (Å), and π-Delocalization Parameters, $Q = d_1 - d_2 + d_3 - d_4$ (Å) and $\lambda_{Q,\mathrm{exp}} = (1 - Q/0.32)/2$ at 100 K[a]

cmpd		O···O	O–H	H–O	O–H–O	p (%)	d_1	d_2	d_3	d_4	Q	$\lambda_{Q,\mathrm{exp}}$
A (100 K)		2.434(1)	1.15(3)	1.32(3)	159(2)	100	1.307(1)	1.388(1)	1.418(1)	1.292(1)	0.045	0.43
B (100 K)												
	a:	2.573(1)	0.84(3)	1.75(3)	170(3)	59(3)	1.297(1)	1.399(1)	1.417(1)	1.280(1)	0.035	0.45
	a′:		0.85(4)	1.75(4)	165(4)	41(3)						
	b:	2.618(1)	0.85(3)	1.79(3)	164(3)	59(3)	1.300(1)	1.400(1)	1.413(1)	1.278(1)	0.035	0.45
	b′:		0.84(4)	1.81(4)	160(4)	41(3)						
C (100 K)												
	a:	2.558(1)	0.89(2)	1.75(2)	150(2)	80(3)	1.333(1)	1.365(2)	1.440(2)	1.247(1)	0.161	0.25
	a′:		0.88(6)	1.72(7)	160(6)	20(3)						

[a] Standard deviations in parentheses; symbols *a* and *b* indicate the two moieties $HO_1-C_2=C_1-C_6=O_2$ and $HO_3-C_{10}=C_9-C_{14}=O_4$ of compound B, while the pairs *a*, *a*′ and *b*, *b*′ indicate couples of tautomeric −O−H···O═ and ═O···H−O− H− bonds.

corresponding to PT-pathways **2**, **2a**,**b** and **3** or **1** and **1a**,**b**, respectively.

The intrinsic PT-pathways (scheme **III**) can be: (**1**) true SM/sSW-NB and (**2**) DM/sSW-NB with no barrier to cross, which are indistinguishable by diffraction methods (if not for the shape of the proton thermal ellipsoid); (**3**) DM/sDW-LB with low-barrier and dynamic crystalline disorder; and (**4**) DM/sDW-HB with a higher PT-barrier that is not crossed at the experimental temperature, thus giving statically disordered crystals. Slight dissymmetrization of the profiles **1** and **2** due to inhomogeneities of the crystal-field forces and/or to slightly dissymmetric substituents does not change the SW nature of the profile except for a slight off-centering of the proton (see schemes **IV** and **V**). More complex is the effect produced by dissymmetrization of profile **4** (scheme **VI**). The increasing value of $\Delta\mathrm{PA}/\Delta\mathrm{p}K_a = \Delta E_{1-2}$ increasingly weakens the two H-bonds formed and, at the same time, splits them in a lower energy, and then more stable, O−H···O (on the left) and a higher-energy, and then less stable, O···H−O bond (on the right). Interpretation relies on (i) the Hammond postulate[9a] stating that the closer a minimum is to the transition-state (TS) position, the more it participates of its geometrical structure and (ii) the concept that the H-bond formed at the TS is always the strongest, most symmetric and covalent possible for any H-bonded molecular system.[2d] Accordingly, the ΔE_{1-2} increase makes the more stable O−H···O bond weaker and weaker because it is increasingly farther from the TS, transforming the rather strong and symmetric DW H-bond **4** into a weaker asymmetric DW with $p_1 > p_2$ (**4a**,**b**) and, finally, into a very weak and asymmetric SW bond (**4c**,**d**) whose upper-level O···H−O counterpart is no longer accessible. Rather paradoxically, the higher-energy bond, which can be calculated theoretically but not observed experimentally, would become stronger and stronger because it is closer and closer to the TS structure.

Analysis of the Crystal Structures

Generalities. Complete experimental details and tables of results for compounds **A**−**C** at the different temperatures investigated are deposited as Supporting Information. H-bond geometries and selected bond distances, percent H-bond proton populations, p(%), and π-delocalization parameters (Q and λ_Q: see below) for compounds **A**−**C** at 100 K are given in Table 1, while data at all temperatures are deposited as Table S1. ORTEP[13] views of the molecular structures at 100 K are given in Figures 1a, 2a, and 3a for **A**, **B**, and **C**, respectively. ORTEP[13] views at all temperatures are deposited as Figures S1−S3. Figures 1b and 3b display the difference Fourier maps computed in the mean plane of the H-bonded chelate ring for compounds **A** and **C** at 100 K. Panels b−e of Figure 2 display similar maps projected on the mean plane of the four H-bonded oxygen atoms for compound **B** at 100, 125, 170, and 295 K. All maps were computed after least-squares refinement carried out with the exclusion of the H-bonded hydrogen. Difference Fourier maps for **A** and **C** at all temperatures are deposited as Figures S4 and S5.

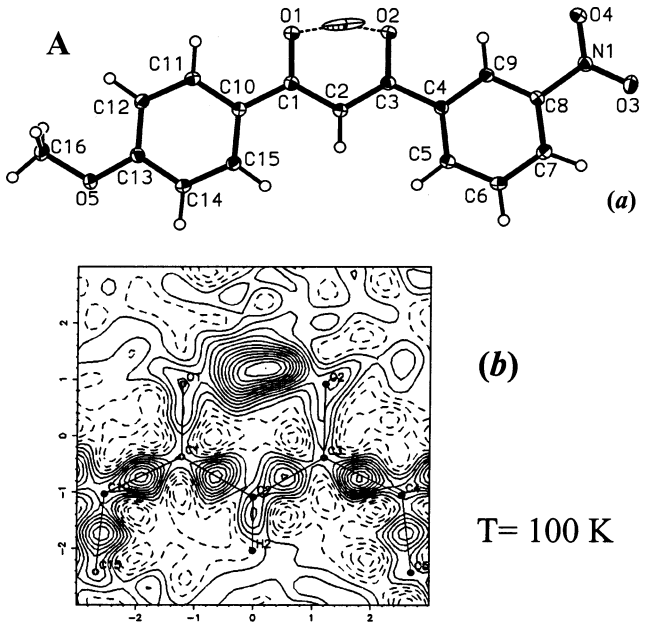

Figure 1. (a) ORTEP[13] view of the molecular structure of compound **A** as determined at 100 K. Thermal ellipsoids are drawn at 40% probability. (b) Difference Fourier map in the mean plane of the H-bond chelate ring for compound **A** at the temperature of 100 K. The map was computed after least-squares refinement carried out excluding the H-bonded hydrogen. Positive (continuous) and negative (dashed) contours drawn at 0.04 e/Å^3 intervals.

Some parameters of Table 1 need further explanation. RAHBs are characterized by a synergistic interplay between H-bond strengthening and increasing delocalization of the π-conjugated fragment connecting the H-bond donor and acceptor atoms. This confers to RAHBs specific geometric features which must be quantified by suitable geometrical descriptors. Making reference to the β-diketone enol **IIb**, the H-bond strength can be measured by the O···O contact distance and the π-delocalization of the ···O═C−C═C−OH··· resonant group by the

(12) (a) Frey, P. A. *Magn. Reson. Chem.* **2001**, *39*, S190. (b) Cleland, W. W. *Biochemistry* **1992**, *31*, 317. (c) Cleland, W. W.; Kreevoy, M. M. *Science* **1994**, *264*, 1887. (d) Frey, P. A.; Whitt, S. A.; Tobin, J. B. *Science* **1994**, *264*, 1927. (e) Cleland, W. W.; Frey, P. A.; Gerlt, J. A. *J. Biol. Chem.* **1998**, *273*, 25529. (f) Harris, T. K.; Mildvan, A. S. *Proteins* **1999**, *35*, 275.

(13) Burnett, M. N.; Johnson, C. K. *ORTEP-III: Oak Ridge Thermal Ellipsoids Plot Program for Crystal Structure Illustrations*, Oak Ridge National Laboratory Report ORNL-6895, TN, 1996.

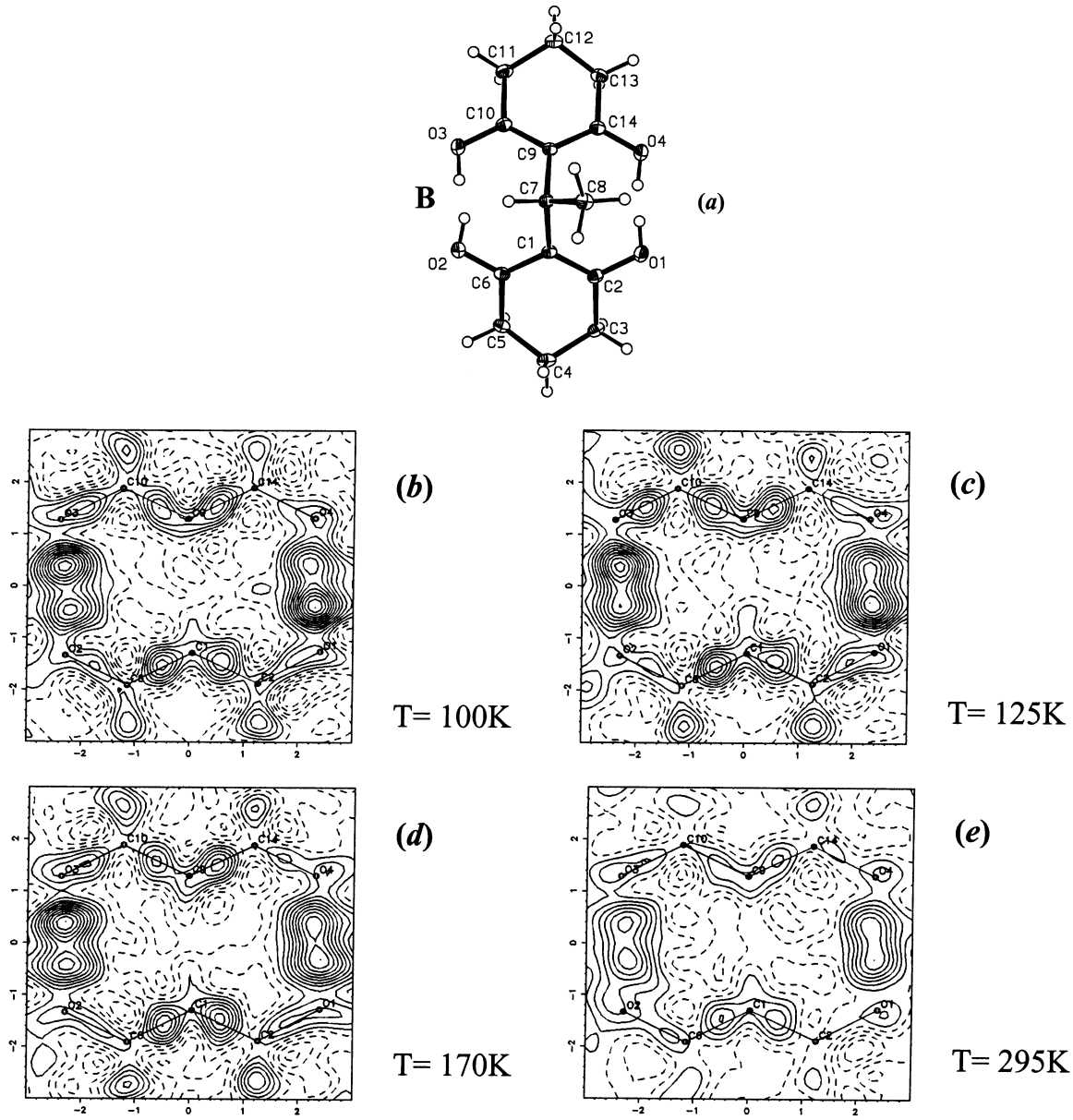

Figure 2. (a) ORTEP[13] view of the molecular structure of compound **B** as determined at 100 K. Thermal ellipsoids are drawn at 40% probability. In the two disordered H-bonds, $O_2-(H)\cdots(H)-O_3$ and $O_1-(H)\cdots(H)-O_4$, both partial proton positions are shown. (b−e) Difference Fourier maps in the mean plane of the four oxygen atoms for compound **B** at the temperatures of 100, 125, 170, and 295 K. The maps were computed after least-squares refinement carried out excluding the H-bonded hydrogens. Positive (continuous) and negative (dashed) contours drawn at 0.04 e/Å^3 intervals.

antisymmetric vibration parameter $Q = d_1 - d_4 + d_3 - d_2$ which is zero for the totally π-delocalized fragment, and it has been shown to amount to $Q = Q_o = \pm 0.320$ Å for the extreme enol−ketonic (**EK**) and keto−enolic (**KE**) forms.[7a] Alternatively, the π-delocalization parameter $\lambda_Q = (1 - Q/Q_o)/2$ can be used ($\lambda = 0$ for **EK**, 1 for **KE**, and 0.5 for complete π-delocalization). λ_Q is known to be intercorrelated with d(O···O) in O−H···O RAHBs by the equation

$$\lambda_Q = 3.47(3) - 1.25(10)d(\mathrm{O}\cdots\mathrm{O}) \quad (r = 0.89) \qquad (1)$$

derived from linear regression analysis of 38 accurate crystal structures.[7c] The comparison of the λ_Q value computed by eq 1, $\lambda_{Q,\mathrm{calc}}$, with that derived from experimental bond distances, $\lambda_{Q,\mathrm{exp}}$, is called thereafter λ-test and is systematically used to determine if experimental values of $\lambda_{Q,\mathrm{exp}}$ near 0.5 are due to true SW H-bonds or to the overlapping of two dynamically or statically disordered fragments in a DW H-bond characterized by the ···O=C−C=C−OH··· ⇄ ···HO−C=C−C=O·· tautomeric equilibrium.

A second method for distinguishing between these two cases[6e,f,14c] is the Hirshfeld's rigid-bond test[14a,b] which consists of computing, for any pair of A and B atoms, the quantity $\Delta\langle u^2\rangle_{A,B} = (U_{ij})_{A,B} - (U_{ij})_{B,A}$ (in Å^2), that is the difference between the anisotropic atomic displacement parameters, U_{ij}, of atoms A and B along the A−B vector. Since chemical bonds are fairly rigid, $\Delta\langle u^2\rangle_{A,B}$ for bonded atoms should not exceed 0.0010 Å^2, larger values being a sign of possible static or dynamic disorder within the crystal. The results of such an analysis for compounds **A** and **B** are deposited as Table S2.

Compound A. The crystal structure of compound **A** reveals the formation of a remarkably strong intramolecular O···H···O bond with O···O distances ranging from 2.448(2) at 295 K to 2.434(1) Å at 100 K (Table S1). The proton position, nearly symmetrical at 295 K, slightly moves toward the O_2 atom with the decreasing temperature. Even at

(14) (a) Hirshfeld, F. L. *Acta Crystallogr.* **1976**, *A32*, 239. (b) Rosenfield, R. E., Jr.; Trueblood, K. N.; Dunitz, J. D. *Acta Crystallogr.* **1978**, *A34*, 828. (c) Vila, A. J.; Lagier, C. M.; Olivieri, A. C. *J. Mol. Struct.* **1992**, *274*, 215 and references therein.

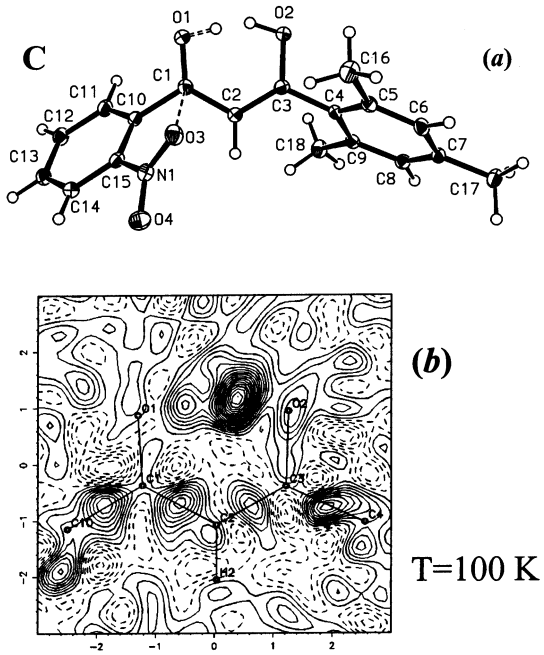

Figure 3. (a) ORTEP[13] view of the molecular structure of compound **C** as determined at 100 K. Thermal ellipsoids are drawn at 40% probability. In the disordered $O_2-(H)\cdots(H)-O_1$ H-bond both partial proton positions are shown. (b) Difference Fourier map in the mean plane of the H-bond chelate ring for compound **C** at the temperature of 100 K. The map was computed after least-squares refinement carried out excluding the H-bonded hydrogen. Positive (continuous) and negative (dashed) contours drawn at 0.04 e/Å^3 intervals.

the lowest temperature, however, there is no sign of disorder, but only indication of a single hydrogen with a high degree of vibrational freedom along the H-bond direction, as illustrated by the strongly anisotropic thermal ellipsoid at 100 K shown in Figure 1a and by the difference Fourier map of Figure 1b showing a single maximum. All data indicate that the H-bond in **A** has the features of a waSW-NB H-bond where the proton experiences a slightly dissymmetrical potential of type **1a** or **2a**. This is confirmed by the $\lambda_{Q,exp}$ of 0.43−0.44, which indicates a nearly 1:1 mixture of the two ···HO−C═C−C═O··· ↔ ···O═C−C═C−OH··· *VB resonant forms*, typical of strong O−H··· O RAHB formation.

Hirshfeld's rigid-bond test for **A** (Table S2) indicates that all bonds are rigid within the expected limit of $\Delta\langle u^2\rangle_{A,B} < 0.0010$ Å^2, with the exception of the two C−O bonds of the β-diketone enol (average $\Delta\langle u^2\rangle_{A,B} \simeq 0.0020[3]$ Å^2). In particular, the rigidity of the two $C_1-C_2-C_3$ bonds indicates that their π-delocalization is really due to resonance, and not to tautomeric disorder. Although with some caution about the reliability of X-ray data,[15] the O···H···O bond picture emerging from present experiments is that of an ordered OCCCO fragment almost completely delocalized by resonance with the two oxygens at a nearly fixed distance ($\Delta\langle u^2\rangle_{O-O} = 0.0004$ Å^2), between which the proton moves freely in a shallow and slightly dissymmetrical single-well potential of type **1a** or, more likely, **2a**. During this large dynamic motion the proton approaches more or less the two oxygens causing small changes of C−O distances of the order of $\Delta\langle d\rangle_{C-O} = (\Delta\langle u^2\rangle_{C-O})^{1/2} \simeq 0.05$ Å at 100 K, not far from those suggested in a previous solid-state ^{13}C NMR study (≃0.10 Å).[14c] Present results are essentially confirmed by a recent charge density study carried out on compound **A** by X-ray diffraction at 110 K.[16]

Compound B. The crystal structure of compound **B** (Figure 2a) shows that the molecule consists of two cyclohexanedione enol subunits linked by an ethylene bridge and two rather strong O−H···O bonds

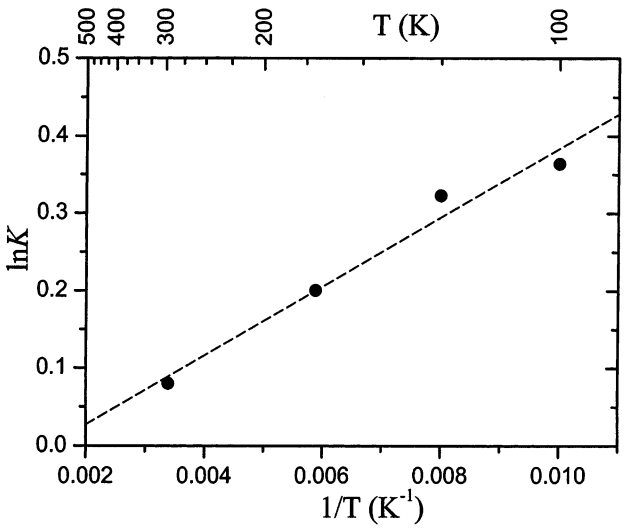

Figure 4. Van't Hoff plot, $\ln K = \Delta S°/R - \Delta H°/R\ (1/T)$, for compound **B**. $K = p/(1-p)$ is the ratio of the proton populations of the two O−H···O and O···H−O tautomers as derived from least-squares refinement. $\Delta H° = -0.088(6)$ kcal mol^{-1}, $\Delta S° = -0.12(4)$ cal K^{-1} mol^{-1} ($n = 8$, $r = 0.987$).

with O···O distances ranging from 2.572(2) and 2.621(2) Å at 295 K to 2.573(1) and 2.618(1) Å at 100 K (Table S1). A number of other similar structures are known[7d,17] which differ in the nature of the bridge or of the cyclohexanedione subunit, all displaying analogous H-bond dissymmetry and comparable O···O distances.

Our first crystal structure determination of this compound at room temperature[7d] resulted in two protons with thermal ellipsoids greatly elongated along the O···O direction, which was interpreted as a case of vibrational disorder within a SW shallow potential. In contrast, least-squares refinement of present more accurate data indicates that the two H-bonds are cases of dynamical proton disorder in a slightly dissymmetrized DW-LB potential of type **3**. This is consistent with the difference Fourier maps b−e of Figure 2 and with the values of percent proton populations, p(%), obtained from the final anisotropic least-squares refinements. These p(%) values slightly change with the temperature from 59:41 at 100 K to 52:48 at room temperature (Table S1) and are essentially identical for both H-bonds. The results can be interpreted in terms of a tautomeric equilibrium between forms **VIIa** and **b**,

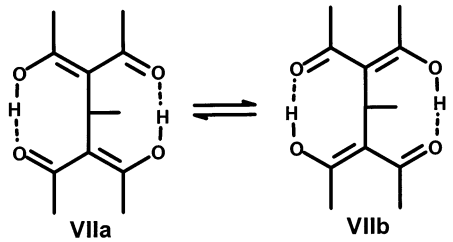

the first being slightly more stable because of being increasingly preferred with the decreasing temperature. This small difference in energy can be evaluated from the van't Hoff plot of Figure 4 to amount to only $\Delta H° = -88(6)$ cal mol^{-1}. The successful application of the van't Hoff method is indicative of a high equilibrium exchange rate and therefore of dynamic proton disorder in the crystal.

Since the actual crystal structure is an almost 1:1 overlapping of *tautomers* **VIIa** and **b**, the disorder should involve also the carbon and oxygen atoms of the enolone fragments. Although this disorder is too

(15) Koritsanszky, T. S.; Coppens, P. *Chem. Rev.* **2001**, *101*, 1583.
(16) Souhassou, M.; Pretto, L.; Gilli, P. Private communication.
(17) (a) Bolte, M.; Scholtyssik, M.. *Acta Crystallogr.* **1997**, *C53*, 1869. (b) Bolte, M.; Degen, A.; Rühl, S. *Acta Crystallogr.* **1997**, *C53*, 340. (c) SethuSankar, K.; Banumathi, S.; Krishna, R.; Velmurugan, D. *Acta Crystallogr.* **2000**, *C56*, e479. (e) Bolte, M.; Degen, A.; Rühl, S. *Acta Crystallogr.* **2001**, *C57*, 446.

small to be detected by either Fourier difference maps (Figure 2b−e) or final least-squares refinement, it can be shown to occur in three different ways: (i) Application of the λ-test at 100 K shows that the $\lambda_{Q,\mathrm{exp}}$ value of 0.45 does not match the $\lambda_{Q,\mathrm{calc}}$ values of 0.25 and 0.20 calculated by eq 1 from the two O···O distances of 2.573 and 2.618 Å, respectively. This seems a clear indication of disorder between the two weakly delocalized tautomers **VIIa** and **b**, whose superimposition simulates a heavily delocalized average one. (ii) Similar results are obtained from the Hirshfeld's rigid-bond test (Table S2), showing that, while the $\Delta\langle u^2\rangle_{\mathrm{A,B}}$ values for atoms outside the resonant fragments average to 0.0006 Å^2 (smaller than the accepted limit of 0.0010 Å^2 for rigid bonds), those for the enolone C and O atoms are much higher, being in the range 0.0028−0.0032 and 0.0019−0.0027 Å^2 for C−O and C−C bonds, respectively. This indicates that, on average, the bond distances of the two tautomeric fragments may differ by $\Delta\langle d\rangle_{\mathrm{A-B}} = (0.0026\ \text{Å}^2)^{1/2} = 0.051$ Å, a value not far from that evaluated by Boese et al. for the disordered DW RAHB in acetylacetone.[6e] (iii) This suggested to try a least-squares constrained refinement based on a model of four identical enolone fragments having fixed bond distances compatible with the small $\lambda_{Q,\mathrm{calc}}$ of 0.20−0.25 given above and occupying (grouped two-by-two and head-to-tail according to **VII**) the positions of the two β-diketone moieties. This constrained refinement has been successful, as detailed in the Supporting Information (page S2), confirming the results obtained by the other two tests.

In summary, all results agree in indicating that the two H-bonds in **B** are to be classified as waDW-LB H-bonds with continuous dynamical O−H···O/O···H−O exchange even in the solid state at 100 K due to the tautomeric equilibrium **VIIa** $\rightleftarrows$ **VIIb**.

Compound C. The molecular structure of compound **C** at 100 K is shown in Figure 3a, and relevant geometrical parameters at the four temperatures investigated are given in Table S1. It differs from the other dibenzoylmethane enol **A** for having both ortho-substituted phenyls out of the plane of the H-bonded resonant fragment. The O−H···O bond formed (O···O = 2.558(1) Å at 100 K) is much weaker than in **A**, and in effect, it is one of the longest ever found in intramolecularly H-bonded β-diketone enols (2.37 ≤ O···O ≤ 2.59 Å; average value = 2.46[4] Å).[2a,b,7e,f] The weakening is imputable to the strong donor−acceptor interaction between the O_3 oxygen of the nitro group and the C_1 atom of the enolone moiety ($C_1\cdots O_3 = 2.732(2)$ Å against a C···O van der Waals distance of 3.22 Å)[18] which makes strongly dissymmetric the resonant fragment and hinders the PA/pK_a equalization normally produced by RAHB. The H-bonded proton is disordered with percent populations of the two partial hydrogens bonded to O_2 and O_1 in the ratio 80:20 at 100 K (Table 1) which do not essentially change with the increase of temperature up to to 295 K (Table S1). The uneven occupation of the two positions is clearly shown in the difference Fourier map of Figure 3b. The H-bond observed is consistent with the aDW-HB PT-pathways **4a** or **4b** having, on both sides, energy barriers, $\Delta E^{\ddagger}_1$ and $\Delta E^{\ddagger}_2$, large enough to avoid easy PT-barrier crossing up to room temperature. This would explain why proton populations are insensitive to temperature and suggests that the observed disorder is static in nature. The π-delocalization parameter of the resonant O═C−C═C−OH keto−enolic fragment ($\lambda_{Q,\mathrm{exp}} = 0.25$) perfectly fits the $\lambda_{Q,\mathrm{calc}}$ of 0.27 calculated by eq 1 for the observed O···O distance of 2.558 Å.

Possibility of Experimental Discrimination between SW and DW H−Bonds. The discrimination between SW and DW H-bonds by X-ray and even neutron crystallography has turned out to be a not simple problem. Convincing experimental evidence of nearly proton-centered SW H-bonds has been obtained only for very few O···H···O and N···H···O (±)CAHBs[6a−d] and a small number of O···H···O (−)-CAHBs[3b−d] or (+)CAHBs,[3g,h] while all proposed cases of proton-centered N···H···N (+)CAHBs were shown to be DW-LB H-bonds by isotopic-perturbation NMR techniques.[19a]

In the case of RAHB the existence of SW bonds has not been definitely assessed thus far even for the shortest HBs observed. The problem is reexamined here by taking advantage of (a) a new *prior* (**III**−**VI**) defining, hopefully, all the possible shapes that PT-barriers can assume, and (b) the general relationships between H-bond strength and π-delocalization typical of RAHB that should, at least in principle, help to discriminate between SW and DW cases. The methods used for attaining such a discrimination are: (i) difference Fourier map in the proton region (DFM); (ii) least-squares refinement of the H-bond proton populations, p (p-LS); (iii) Hirshfeld's rigid-bond test[14a,b] on the C−C−C bonds of the resonant spacer (HRB); (iv) rigid-body least-squares refinement of two superimposed tautomeric fragments (RB-LS); (v) λ-test, i.e. comparison of the experimental π-delocalization indices, $\lambda_{Q,\mathrm{exp}}$, with those calculated from eq 1, $\lambda_{Q,\mathrm{calc}}(\lambda T)$; (vi) dynamic−static test based on the van't Hoff plot $\ln K = \ln p/(1-p)$ versus $(1/T)$ (v'tH). The results of these tests are summarized in Table 2 for compounds **A**−**C** and for a small number of other structures of H-bonded β-diketone enols of high experimental standard determined by microwave spectroscopy (malondialdehyde, MDA)[6g] and neutron (dibenzoylmethane, DBM,[6h] and nitromalondiamide, NMD[6f]) or X-ray diffraction (acetylacetone, ACAC).[6e] The tests give consistent indications for each compound, that is sDW-LB for MDA and ACAC, waDW-LB for **B**, aDW-HB for **C**, and waSW-NB for DBM, NMD and **A**. Dynamic tautomeric exchange in the gas phase or in the crystal is verified for MDA and **B**, respectively. Dynamic exchange in ACAC is suggested by the authors[6e] although it remains essentially indecidable because the crystallographic symmetry between the two tautomers makes proton populations independent of temperature. The PT-pathways suggested by experiments are given in the last column of Table 2 according to the nomenclature summarized in schemes **III**−**VI**.

The results obtained allow us to conclude that (i) the use of a reasonable *prior*, such as that depicted in **III**−**VI**, can certainly help to rationalize and improve experimental data interpretation, and (ii) crystallographic methods are fairly able to assess the shapes of the H-bond PT-barriers in the solid state and, in case of disorder, its dynamic or static nature, in analogy with, but from a different point of view of, NMR techniques of isotopic perturbation in solution.[19]

Application to H-Bond Theory and Generalization

The understanding of RAHBs presents some objective difficulties because of their intimate mixing of covalent and electrostatic contributions, on one side, and of resonance and tautomery, on the other. This can be illustrated for the specific O−H···O case by representing the observed molecular states as a combination of four VB wave functions (sketched at the four corners of Figure 5a) according to the equations[2d]

$$\Psi(\mathrm{O-H\cdots O}) = a\,\Psi(\mathbf{EK}) + b\,\Psi(\mathbf{KE}) + b^{\pm}\,\Psi(\mathbf{EK}^{\pm}) \quad (2a)$$

$$\Psi(\mathrm{O\cdots H-O}) = b\,\Psi(\mathbf{KE}) + a\,\Psi(\mathbf{EK}) + a^{\pm}\,\Psi(\mathbf{KE}^{\pm}) \quad (2b)$$

Only the first of these equations needs to be considered because of the symmetry of the enolone fragment, and Table 3 reports the values of the mixing coefficients a, b, and $b^{\pm}$ of eq 2a calculated for the compounds of Table 2 according to a method previously described.[20] Clearly, the more the H-bond becomes similar to a three-center-four-electron covalent bond,[2a] the more a and b become alike and $b^{\pm}$ tends to zero. The three SW-NB H-bonds (DBM, NMD and **A**) appear to fulfill this condition being, on average, a 56:41 mixture of **EK** and **KE** forms with

(18) Bondi, A. *J. Phys. Chem.* **1964**, *68*, 441.

(19) (a) Perrin, C. L.; Ohta, B. K. *J. Am. Chem. Soc.* **2001**, *123*, 6520. (b) Perrin, C. L. *Science* **1994**, *266*, 1665. (c) Perrin, C. L.; Kim, Y.-J. *J. Am. Chem. Soc.* **1998**, *120*, 12641. (d) Perrin, C. L.; Ohta, B. K. *Bioorg. Chem.* **2002**, *30*, 3.

(20) The method for calculating a, b, and $b^{\pm}$ coefficients from the *RC* versus λ_Q plot of Figure 5a is described in note 21 of ref 2d.

Table 2. H-Bond Classification According to Tests i−vi (See Text) for a Number of Accurate Structures of β-Diketone Enols Forming Intramolecular O−H···O RAHBs: (i) DFM = Difference Fourier Map; (ii) *p*-LS = Proton Population Least-Squares; (iii) HRB = Hirshfeld's Rigid-Bond Test; (iv) RB-LS = Rigid-Body Least-Squares; (v) $\lambda T = \lambda$-Test; (vi) v'tH = van't Hoff Plot[a]

															all tests
				(i) DFM	(ii) *p*-LS		(iii) HRB		(iv) RB-LS	(v) λT			(vi) v'tH		final
cmpd	structure determination	O···O (Å)	*RC* (Å)	result	*p*/(1-*p*) (%)	result	$\Delta\langle u^2\rangle_{A,B}$[c] (Å$^2\times10^4$)	result	result	$\lambda_{Q,exp}$ (%)	$\lambda_{Q,calc}$ (%)	result	result		H–bond classification
MDA	MW[d]	2.553	±0.77[b]	−	50/50	sDW	−	−	−	20/80	28/72	DW	dynamic (LB)[d,e]		sDW-LB (**3**)
ACAC	X (110 K)	2.547(1)	±0.79[b]	sDW	50/50	sDW	31	DW	−	50	28/72	DW	dynamic (LB)[e]		sDW-LB (**3**)
B	X (100 K)	2.573(1)	±0.77[b]	waDW	59/41	waDW	21	DW	DW	44	25/75	DW	dynamic (LB)		waDW-LB (∼**3**)
		2.618(1)	±0.72[b]	waDW	59/41	waDW	25	DW	DW	44	20/80	DW	dynamic (LB)		waDW-LB (∼**3**)
C	X (100 K)	2.558(2)	±0.75[b]	aDW	80/20	aDW	15	DW	−	25/75	27/73	DW	static (HB)		aDW-HB (**4a,b**)
DBM	N (rt)	2.459(4)	0.20(2)	waSW	100	SW	−	−	−	40	40	SW	ordered (NB)		waSW-NB (**2a**)
NMD	N (15 K)	2.391(3)	0.17(1)	waSW	100	SW	<10	SW	−	49	48	SW	ordered (NB)		waSW-NB (**1a**)
A	X (100 K)	2.434(1)	0.17(3)	waSW	100	SW	<10	SW	−	43	43	SW	ordered (NB)		waSW-NB (**2a**)

[a] Compounds: MDA = malondialdehyde;[6g] ACAC = acetylacetone;[6e] DBM = dibenzoylmethane;[6h] NMD = nitromalondiamide.[6f] $RC = [d(O-H) - d(H\cdots O)]$ = reaction coordinate; p = H-bond proton population; $\Delta\langle u^2\rangle_{A,B} = U_{ij}$ difference along the A−B bond; $\lambda_{Q,exp}$ and $\lambda_{Q,calc}$ = experimental and calculated π-delocalization parameters; MW = microwave spectroscopy; X and N = X-ray and neutron crystallography; SW and DW = single and double well; NB, LB, and HB = no-, low-, and high-barrier; s, a, and wa = symmetric, asymmetric, and weakly asymmetric. [b] O−H distances < 0.94 Å normalized to 0.94 Å. [c] Average of the values for the two C−C bonds of the enolone fragment. [d] In the gas phase. [e] Estimated by the authors by non-van't Hoff methods.

a small contribution of the charged form **EK**$^{\pm}$. To notice, however, that the mixture is not exactly 50:50, indicating that the complete PA/pK_a matching is never reached (at least in this limited series of compounds) because of insufficient delocalization of the π-conjugated system (cfr **IIb**). Very different is the situation for DW-LB H-bonds (MDA, ACAC, and **B**) whose a:b:$b^{\pm}$ ratio is near to 75:12:13, indicative of a weaker perturbation of the **EK** form by nearly identical contributions of the neutral **KE** and charged **EK**$^{\pm}$ forms.

Since the mixing **EK**↔**KE**$^{\pm}$ and **KE**↔**EK**$^{\pm}$ changes $RC = [d(O-H) - d(H\cdots O)]$ without affecting the π-delocalization, while the mixing of **EK**↔**EK**$^{\pm}$ and **KE**↔**KE**$^{\pm}$ modifies the π-delocalization index, λ_Q, but not the O−H···O geometry, the resonance depicted by eqs 2, a and b, can be represented in the space spanned by RC and λ_Q which are both accessible from experiments. This type of plot[2d,7a] is shown in Figure 5a, while the parallel plot reporting the O···O contact distances as a function of λ_Q is given in Figure 5b. The data set used has been extended to include 34 more crystal structures of good accuracy derived from a CSD[10] search over all H-bonded β-diketone enol derivatives not fused with other rings (the complete list is available as Table S3 of the Supporting Information). Symbols employed are open squares, open triangles, and open circles for molecules forming SW, DW, and aSW H-bonds, respectively. Superimposed small full points mark the compounds listed in Table 2, while diagonal crosses indicate the incorrect positions assumed by DW H-bonds misinterpreted as SW ones because their large $\lambda_{Q,exp}$ values were erroneously attributed to almost complete π-delocalization instead of the geometrical average of two less-delocalized and antidromic O=C−C=C−OH and HO−C=C−C=O tautomeric groups. Both plots of Figure 5 clearly show that the mispositioning of points due to mistaking DW for SW H-bonds is very large and such to impair the d(O···O) versus λ_Q correlation typical of RAHB.[21]

Chemical formulas of all compounds considered are summarized in schemes **VIII** and **IX**.

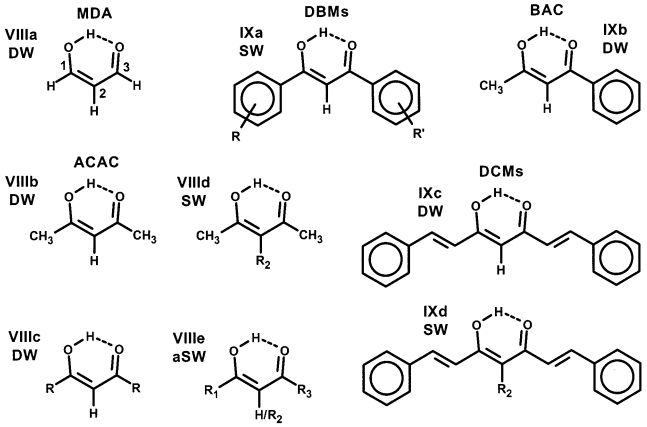

Some regularities appear evident. Symmetric and weakly hindered molecules such as MDA (**VIIIa**), ACAC (**VIIIb**), and other symmetrically substituted enolones ($R_1 = R_3$) having R_2 = H (**VIIIc**) give rise to sDW-LB H-bonds (**III**: **3**), while those sterically constrained by the 2-substituent (**VIIId**) produce much shorter and weakly asymmetric waSW-NB H-bonds (**IV**: **1a**,**b** or **V**: **2a**,**b**). Conversely, all nonsymmetrical 1,3-substituted enolones (**VIIIe**) give aSW-HB H-bonds (**VI**: **4c**,**d**), irrespectively of the 2-substituent. The same effects are observed in dicinnamoylmetane derivatives[22] (DCMs), a class of symmetrical molecules forming sDW-LB H-bonds when R_2 = H (**IXc**)[22e] and waSW-NB H-bonds for $R_2 \neq$ H (**IXd**). Slightly different is the case of DBM derivatives (**IXa**) which are found to easily form waSW-NB H-bonds even if R_2 = H and when

(21) To avoid this type of error, all structures reported in Figure 5 as examples of SW-NB H-bonds (open squares) have been selected among those having a $\Delta\lambda = |\lambda_{Q,exp} - \lambda_{Q,calc}|$ not greater than 0.06.

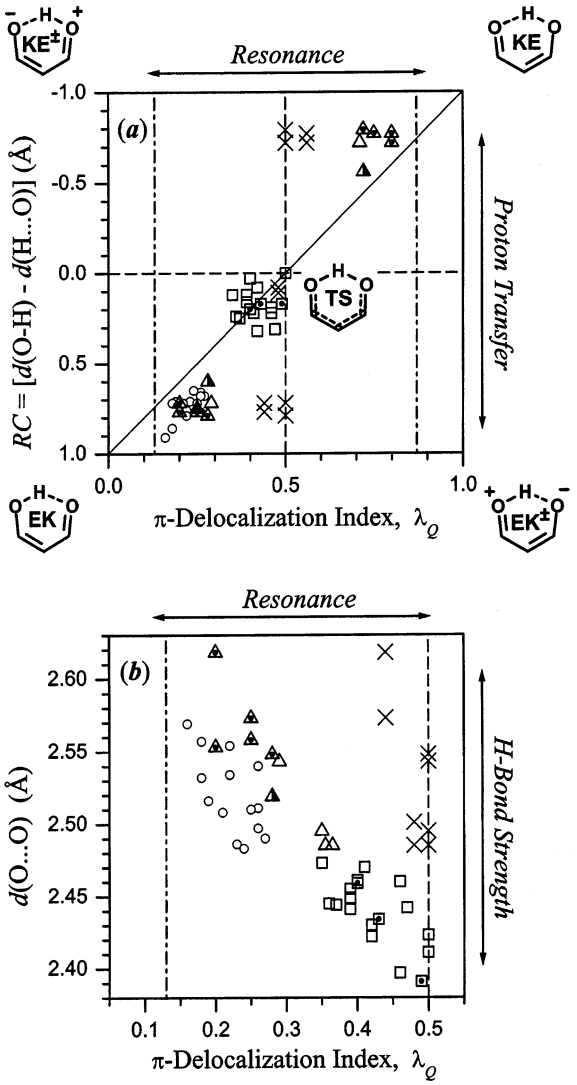

Figure 5. (a) PT-reaction coordinate $RC = [d(O-H) - d(H\cdots O)]$ (Å) and (b) O···O contact distance (Å) plotted against the π-delocalization index λ_Q for a number of crystal structures of β-diketone enols forming intramolecular O−H···O RAHBs. Open squares (□), open triangles (△), and open circles (○) indicate SW-NB, DW-LB, and aSW-HB H-bonds, respectively. Compounds of Table 2 are marked by a superimposed smaller full point (•). Diagonal crosses (×) along the vertical line at $\lambda_Q = 0.5$ mark the incorrect positions assumed by DW H-bonds when the tautomeric disorder is misinterpreted. Noncrystallographic DFT-optimized geometries are shown by triangular half-filled symbols. The two vertical dash−dot lines at $\lambda_Q = 0.13$ and 0.87 indicate the normal enolone π-delocalization in its non-H-bonded state.[7a]

the substituents on the two phenyl groups are not identical, an apparent anomaly which may be accounted for by the strict range of pK_a values (3−5)[23] of monosubstituted benzoic acids. Finally, there has been much debate on the nonsymmetric structure of benzoylacetone (BAC; **IXb**) which was classified as SW by low-temperature X-ray and neutron crystallography[3e], though DFT calculations at the B3LYP/6-311G(d,p) level of theory[3f] showed a rather low DW barrier. The authors suggested

(22) (a) Mostad, A.; Pedersen, U.; Rasmusson, P. B.; Lawesson, S.-O. *Acta Chem. Scand.* **1983**, *B37*, 901. (b) Mostad, A.; Pedersen, U.; Rasmussen, P. B.; Lawesson, S.-O. *Acta Chem. Scand.* **1984**, *B38*, 479. (c) Görbitz, C. H.; Mostad, A.; Pedersen, U.; Rasmussen, P. B.; Lawesson, S.-O. *Acta Chem. Scand.* **1986**, *B40*, 420. (d) Görbitz, C. H.; Mostad, A. *Acta Chem. Scand.* **1993**, *47*, 509. (e) Compound of ref 22a has been classified as SW-NB by the authors and DW-LB by ourselves.

(23) *CRC Handbook of Chemistry and Physics*, 75th ed.; Lide, D. R., Frederikse, H. P. R., Eds.; CRC Press: Boca Raton, FL, 1994; pp 8−45.

Table 3. VB Mixing Coefficients a, b, and $b^{\pm}$ (Normalized as $a + b + b^{\pm} = 100$) of the Three **EK**, **KE**, and **EK**$^{\pm}$ Canonical Forms of Equation 2a for the O−H···O Bonds Formed by the Compounds Listed in Table 2[a]

cmpd	H-bond type	a (×100)	b (×100)	$b^{\pm}$ (×100)
MDA	DW-LB	80	11	9
ACAC	DW-LB	72	11	17
B	DW-LB	71	14	15
	DW-LB	75	12	13
C	DW−HB	75	12	13
DBM	SW−NB	60	40	0
NMD	SW−NB	51	42	7
A	SW−NB	57	42	1

[a] For DW H-bonds, the O−H···O bond is mirrored by an identical O···H−O one having coefficients (eq 2b) $b = a$, $a = b$, and $a^{\pm} = b^{\pm}$.

a waSW-NB H-bond with a PT-barrier lower than the zero-vibrational level of the proton, while we would rather suggest a disordered waDW-LB H-bond because the molecule does not meet the requirement of the λ-test, displaying a $\lambda_{Q,\mathrm{exp}}$ of 0.48 against $\lambda_{Q,\mathrm{calc}}$ of 0.34 and 0.28, calculated by eq 1 from the experimental d(O···O)[3e] or from the C−C and C−O distances of the DFT-emulated geometry,[3f] respectively.

It can be concluded that, as a rule, only the 1,3-symmetrically substituted enolones that can match the principle of PA/pK_a equalization can give rise to DW-LB H-bonds that can, in turn, switch to stronger SW-NB ones because of the slight compression exerted by 2-substitution. The only compounds which seem able to form SW-NB H-bonds without the assistance of 2-substituents are DBM derivatives (**IXa**). A reason for that might be the slight repulsion between the two phenyls and the central H-bonded ring, although it seems equally reasonable to relate the ease by which DBMs form SW-NB H-bonds to the increased π-bond delocalizability arising from the two aromatic substituents, which could also account for the fact that BAC gives a DW-LB H-bond at variance with all other dissymmetric enolones **VIIIe** forming aSW-HB ones. The three types of H-bonds observed display strictly contiguous metric and bonding properties

$$\text{waSW-NB: } 2.39 \le d(\mathrm{O\cdots O}) \le 2.47 \text{ Å}; \quad 0.49 \ge \lambda_{Q,\mathrm{exp}} \ge 0.35$$

$$\text{average } a{:}b{:}b^{\pm} = 56[5]{:}40[5]{:}4[4]$$

$$\text{sDW-LB: } 2.48 \le d(\mathrm{O\cdots O}) \le 2.55 \text{ Å};$$
$$0.36 \ge \lambda_{Q,\mathrm{calc}} \ge 0.20 \text{ and } 0.64 \le \lambda_{Q,\mathrm{calc}} \le 0.80$$

$$\text{average } a{:}b{:}b^{\pm} = 75[4]{:}13[3]{:}12[4]$$

$$\text{aSW-HB: } 2.48 \le d(\mathrm{O\cdots O}) \le 2.57 \text{ Å}; \quad 0.27 \ge \lambda_{Q,\mathrm{exp}} \ge 0.16$$

$$\text{average } a{:}b{:}b^{\pm} = 77[4]{:}14[3]{:}9[3]$$

showing that very short O···O distances are always associated with mostly covalent waSW-NB H-bonds, while the other two classes (sDW-LB and aSW-HB) have rather similar distances and bonding properties and differ only for the degree of π-delocalization of the resonant fragment which is slightly greater for DW-LB tautomeric pairs.

It seems important to associate each H-bond type to a reasonable estimate of the energies involved, E_{HB}. These have been evaluated by DFT methods at the B3LYP/6-31+ G(d,p)// B3LYP/6-31+G(d,p) level (see Supporting Information) by comparing the energies of the H-bonded and non-H-bonded (or

open) forms, the latter being obtained by 180° rotation of the hydroxyl group around the C−OH bond. Calculations have been performed for the β-diketones DBM and MDA and for the β-ketoester HAA (3-hydroxyacrylic acid) as typical examples of molecules forming SW-NB, DW-LB and aSW-HB H-bonds. Calculated E_{HB} values were respectively 19.84, 13.56, and 13.59 kcal mol^{-1} (decreasing by some 0.5 kcal mol^{-1} after zero-point correction) for O···O distances of 2.475, 2.569, and 2.592 Å, showing again the close similarity of DW-LB and aSW-HB H-bonds in the O−H···O RAHB system.

Conclusions

The factors affecting O−H···O bond strength in β-diketone enols are summarized in Figure 6a in the form of a cybernetic effector diagram. The H-bond strength is seen to be enhanced or reduced by steric forces producing, respectively, compression or stretching of the O···O contact distance but, above all, increased by the PA/pK_a equalization between the O−H and O═C interacting groups prompted by both homonuclearity and molecular symmetry. What is characteristic of RAHB is the presence of the positive (or deviation-amplifying) feedback connecting the effect (H-bond strength) with one of the causes (PA/pK_a equalization) through the π-delocalization of the resonant fragment, π. This triggers the RAHB synergistic mechanism by which H-bond strengthening induces enhanced delocalization that, in turn, causes further strengthening until repulsion exchange stops the process at its equilibrium position. The graph is completed by the dashed arrow marked "aromaticity" which takes into account the contribution of aryl substituents to the π-bond delocalizability of the H-bonded resonant fragment, suggested above for DBM derivatives.

The chemical-bond aspects of RAHB remain, however, to be understood and clarified. Figure 6b is an attempt to do that by means of a state-correlation (or avoided-crossing) diagram[24a] illustrating the ideal PT-pathway of *symmetric* β-diketone enols forming *intrinsic* intramolecular H-bonds. The two ground-state forms **EK** and **KE** have different spin pairing and cannot mix without the intervention of the charge-transfer excited states **EK**$^{\pm}$ and **KE**$^{\pm}$. The PT occurs at the crossing point, where the two states have identical spin pairing and energy, and can then mix, lowering the TS energy (while increasing that of the corresponding excited-state) by ΔE_{RES} that can be regarded as the quantum-mechanical resonance energy of the transition state.[24a] This is small (dashed curve **HB**) for DW-HB, larger for DW-LB (dashed curve **LB**), and much larger for SW-NB H-bonds for which the TS is lowered in such a way as to become the thermodynamically stable form (dashed curve **NB**). This treatment seems, therefore, to indicate that the word "resonance" often used to define RAHB as due to an interplay between H-bond strengthening, and resonance[7a,b] can be given the more precise meaning of TS resonance energy in the avoided-crossing diagram of the H-bond PT process. It makes clear, moreover, that SW-NB H-bonds are to be understood as the bonds having in their ground state the structure displayed by the TS in weaker H-bonds, and that they can become strong and essentially covalent just because they can participate, in a way, of the nature of the TS which is always the strongest three-center-four-electron covalent bond achievable in any H-bonded system.[2d]

(24) (a) Reference 9d and references therein. (b) Haddon, R. C. *J. Am. Chem. Soc.* **1980**, *102*, 1807. (c) Streitwieser, A., Jr. *Molecular Orbital Theory of Organic Chemistry*; Wiley: New York, 1961. (d) Pearson, R. G. *J. Am. Chem. Soc.* **1969**, *91*, 4974.

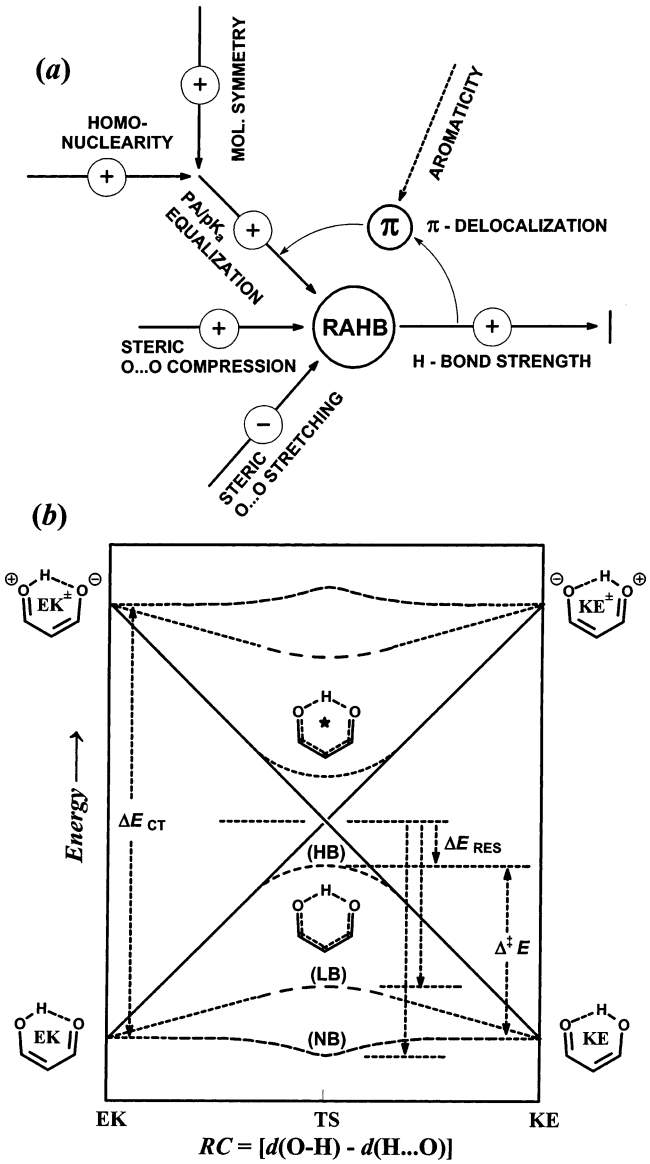

Figure 6. (a) The O−H···O RAHB logic described as a cybernetic effector with positive (i.e., deviation amplifying) feedback connecting backward the H-bond strength (the effect) with the PA/pK_a equalization (one of the input variables) through the π-delocalization of the O═C−C═C−OH enolone fragment, π. (b) State-correlation (or avoided-crossing) diagram[24a] for the PT reaction in intramolecularly H-bonded and symmetrically substituted β-diketone enols. Because of different spin pairing, **EK** and **KE** forms cannot correlate without intervention of the charge-transfer excited states **EK**$^{\pm}$ and **KE**$^{\pm}$ which are higher in energy by ΔE_{CT}. PT occurs at the crossing point where the two states of identical spin pairing and energy can mix by resonance lowering the TS energy by ΔE_{RES} and then decreasing the PT energy barrier $\Delta E^{\ddagger}$. ΔE_{RES} is small for DW-HB H-bonds, larger for DW-LB, and much larger for SW-NB H-bonds for which the TS is transformed into the thermodynamically stable configuration (curves **HB**, **LB**, and **NB**, respectively).

The present interpretation fits the conclusions drawn by Haddon[24b] by applying simple Hückel-MO theory[24c] to the analysis of the factors that may perturb, or less, the fully π-delocalized enolone geometry **IIb**, characteristic of proton-centered sSW-NB H-bonds, by second-order Jahn−Teller effect[24d] prompted by HOMO−LUMO configuration interaction. A large HOMO−LUMO gap was found to be the essential condition for strong and symmetric H-bond formation in complete agreement with the conclusions drawn from the avoided-crossing diagram of Figure 6b.

Acknowledgment. We thank CINECA, Casalecchio di Reno (Bologna), for free use of its IBM SP4 computer facility, and INSTM (Florence) for financial support of our computational activities.

Supporting Information Available: Experimental section, table of structural parameters for compounds **A**−**C**, rigid-bond test for **A** and **B**, structural data for compounds of Figure 5, table of DFT geometries and energies, ORTEP plots for compounds **A**−**C**, and difference Fourier maps for **A** and **C** at all the temperatures (PDF). X-ray crystallographic files (11 CIF files). This material is available free of charge via the Internet at http://pubs.acs.org.

JA030213Z